Localized Molecular Orbitals for Polyatomic Molecules. IV. Large Boron Hydrides

D. A. Dixon, D. A. Kleier, T. A. Halgren, and W. N. Lipscomb*

Contribution from the Department of Chemistry, Harvard University, Cambridge, Massachusetts 02138. *Received May 27, 1975*

Abstract: Wave functions calculated in the approximation of partial retention of diatomic differential overlap (PRDDO) are presented for $B_{13}H_{19}$, $B_{14}H_{20}$, $B_{16}H_{20}$, *n*-$B_{18}H_{22}$, *i*-$B_{18}H_{22}$, $B_{20}H_{16}$, $B_{20}H_{18}^{2-}$, and photo-$B_{20}H_{18}^{2-}$. The wave functions are analyzed in terms of the ground state charge distribution. Atomic and group charges, inner-shell eigenvalues on boron, dipole moments, and ionization potentials are presented for these molecules. We make and then compare reactivity predictions for electrophilic and nucleophilic attack based on group charges and inner-shell eigenvalues, neglecting steric effects, orbital control, and complex pathways. Localized molecular orbitals (LMO's) obtained using the Boys criterion are reported. These LMO structures are compared with the LMO structures obtained for the B_8 or B_{10} molecules that join together to give the larger molecule. The effects of the bonding in the fusion or bridge region are examined.

The boron hydrides have been studied extensively by various theoretical techniques.[1,2] In particular, wave functions and related molecular properties of the smaller boranes have been calculated by ab initio SCF methods.[2] However, due to financial restrictions, $B_{10}H_{14}$ and $B_{10}H_{14}^{2-}$ are the largest boranes studied so far by ab initio methods.[3] In order to obtain wave functions for comparable or larger molecules in reasonable computer times, various approximate methods have been developed.[4] As judged from a comparison of molecular orbital calculations at several levels of approximation, the PRDDO (partial retention of diatomic differential overlap) method has been shown[5] to provide results most closely reproducing ab initio results, using either Slater basis sets or STO-3G basis sets. Accordingly, the PRDDO method is employed here to generate the wave functions for all of the molecules discussed below.

Boron hydrides with more than 12 borons are not known to form simple polyhedral structures, due to geometric restrictions; they are essentially composed of molecular fragments which are joined in a number of different ways. The structures of eight large boron hydrides have been determined by x-ray diffraction techniques.[6-13] Each of these molecules contains at least one B_8 fragment resembling B_8H_{12} or B_{10} fragment resembling $B_{10}H_{10}^{2-}$, $B_{10}H_{14}$, or $B_{10}H_{14}^{2-}$ (Figure 1). Thus, the $B_{13}H_{19}$[6] molecule (Figure 2) is composed of fused B_8 and B_7 fragments, while $B_{14}H_{20}$[7] (Figure 3) is composed of two B_8 fragments. The $B_{16}H_{20}$[8] molecule (Figure 4) is composed of a B_8 fragment and a B_{10} ($B_{10}H_{14}$ like) fragment while *n*-$B_{18}H_{22}$[9] (Figure 5) and *i*-$B_{18}H_{22}$[10] (Figure 6) are composed of two B_{10} ($B_{10}H_{14}$ like) fragments. For these molecules we note that fusion of the fragments occurs with loss of two borons. The $B_{20}H_{16}$[11] molecule (Figure 7) is also composed of two B_{10} fragments bridged together where these fragments resemble $B_{10}H_{14}^{2-}$. The doubly negative ions, $B_{20}H_{18}^{2-}$ (Figure 8) and photo-$B_{20}H_{18}^{2-}$ (Figure 9), are derived from two $B_{10}H_{10}^{2-}$ structures in which boron bridging occurs in the former and hydrogen bridging in the latter.

Nuclear magnetic resonance spectra have been reported for all of these molecules except $B_{16}H_{20}$ and $B_{13}H_{19}$. The $B_{20}H_{18}^{2-}$,[14] photo-$B_{20}H_{18}^{2-}$, $B_{20}H_{16}$,[16] and $B_{14}H_{20}$[7] spectra support the x-ray results while the spectra of the two $B_{18}H_{22}$ isomers[17] have not been well characterized.

Many of the structurally related large boron hydrides have similar synthetic origins. A brief review of the reactions forming these molecules will help to illustrate this point. $B_{20}H_{18}^{2-}$ was the first of the large boranes to be discovered[18] and is formed with 95% yield in aqueous solution by the reaction

$$2B_{10}H_{10}^{2-} + 4Fe^{3+} \rightarrow B_{20}H_{18}^{2-} + 4Fe^{2+} + 2H^+$$

The two $B_{18}H_{22}$ isomers[17] are formed by reaction of $B_{20}H_{18}^{2-}$ with acids, *n*-$B_{18}H_{22}$ being the major product and the thermodynamically less stable *i*-$B_{18}H_{22}$, the minor product. Photo-$B_{20}H_{18}^{2-}$ is formed[20] by photolysis under a mercury lamp of $B_{20}H_{18}^{2-}$ in acetonitrile solution. The $B_{20}H_{16}$ molecule has been prepared[16a] from $B_{10}H_{14}$ and H_2 in an electric discharge, and is also produced in the chain reaction which takes place upon laser excitation of a vibration of B_2H_6.[21] The $B_{16}H_{20}$ molecule is produced[22] in small amounts (7%) from the pyrolysis of $B_9H_{13}S(CH_3)_2$, $B_{10}H_{14}$ and *n*-$B_{18}H_{22}$ being the major products. The $B_{14}H_{20}$ molecule is produced[7] by the reaction of B_8H_{12} with KB_6H_9 in diethyl ether, followed by removal of solvent and treatment with HCl; $B_{16}H_{20}$ is also found as a product of this reaction. The $B_{13}H_{19}$ molecule is a minor product[23] in the pyrolysis of B_6H_{10}.

The molecules $B_{16}H_{20}$,[22] *n*-$B_{18}H_{22}$, and *i*-$B_{18}H_{22}$[17] are all strong acids. By analogy to $B_{10}H_{14}$ it is presumed that certain bridge protons are most acidic. The reactions of the $B_{18}H_{22}$ isomers have been studied in some detail[17] but little work has been reported for the other molecules discussed here.

In order to compare the bonding in these molecules, we examine their localized molecular orbitals[24] (LMO's). These LMO's are generated by a unitary transformation which is applied to the SCF canonical molecular orbitals.[25] The two most commonly used criteria for choosing this transformation are those of Boys[26] and of Edmiston and Ruedenberg[27] (ER). Computationally, application of the Boys and ER criteria are N^3 and N^5 processes, respectively, where N is the number of occupied orbitals. Except for well-noted differences,[25] the LMO's generated using the Boys criterion are essentially qualitatively the same as those obtained using the ER criterion, but application of the Boys criterion is much more economical.

LMO's are especially useful for making comparisons within a series of structurally related molecules[24] since they provide a means for identifying bonding characteristics which are transferable from small molecules to larger molecules in the series. The large molecules studied here are particularly interesting in this respect because they are composed of fragments which are similar in geometry to several smaller boron hydrides.

We have obtained PRDDO wave functions for the eight large boron hydrides: $B_{13}H_{19}$, $B_{14}H_{20}$, $B_{16}H_{20}$, *n*-$B_{18}H_{22}$,

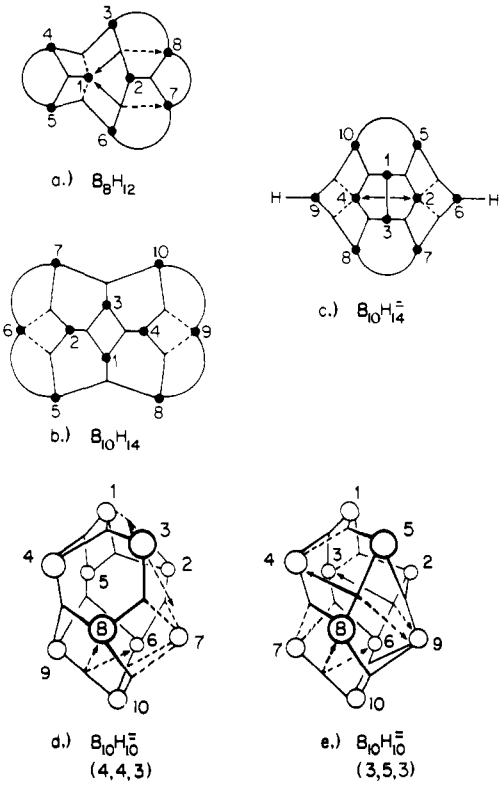

Figure 1. Localized valence structures for the basic fragment type molecules. Bonding conventions from ref 24 are (1) - - - 0.15 to 0.25 e, (2) — 0.25 to 0.35 e, (3) - - - 0.35 to 0.50 e, (4) — population greater than 0.50 e: (a) B_8H_{12}; (b) $B_{10}H_{14}$; (c) $B_{10}H_{14}^{2-}$; (d) 4,4,3 structure of $B_{10}H_{10}^{2-}$; (e) 3,5,3 structure of $B_{10}H_{10}^{2-}$.

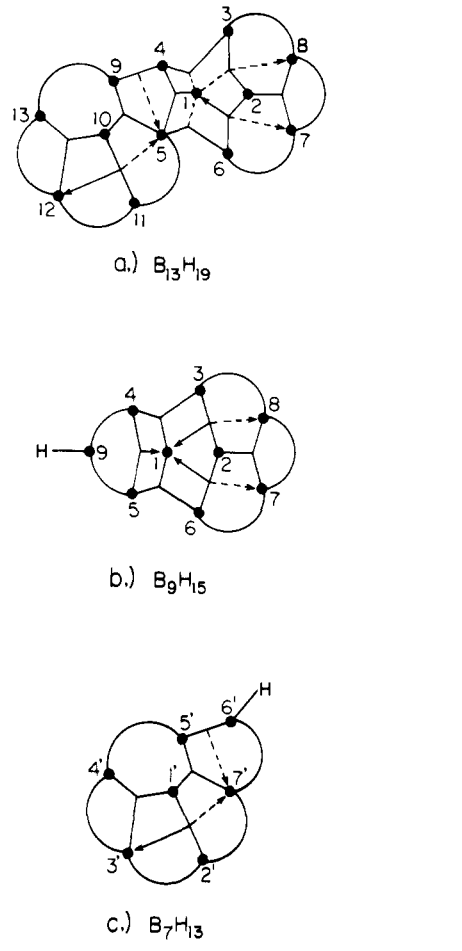

Figure 2. Localized valence structure for $B_{13}H_{19}$: (a) $B_{13}H_{19}$; (b) B_9H_{15} showing its difference from $B_{13}H_{19}$; (c) B_7H_{13}, the valence structure of a postulated boron hydride. Three-dimensional drawing for $B_{13}H_{19}$ is in ref 6.

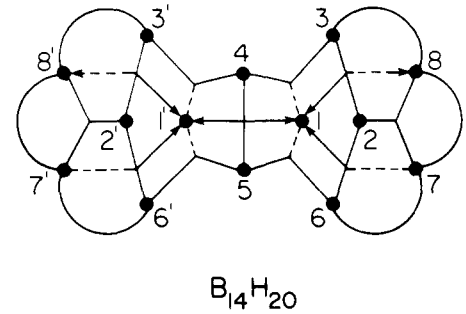

Figure 3. Localized valence structure for $B_{14}H_{20}$. Three-dimensional drawing is in ref 7.

i-$B_{18}H_{22}$, $B_{20}H_{16}$, $B_{20}H_{18}^{2-}$, and photo-$B_{20}H_{18}^{2-}$. We make predictions of the favored sites of electrophilic and nucleophilic attack based on charges and inner-shell eigenvalues on boron.[24] The Boys LMO's are compared with those previously obtained for the smaller fragments.[24,29] Transferability is also discussed.

Calculations and Geometry

The SCF calculations were done with use of the all-electron PRDDO method[5] which employs a minimum basis set of Slater orbitals. Exponents were taken from optimized minimum basis set results for B_2H_6[30] [B(1s), 4.68; B(2s), 1.443; B(2p), 1.477; H_t(1s), 1.147; H_b(1s), 1.209]. Geometries (in Table IV) were based upon the crystal structure results, except that all terminal hydrogen positions were idealized to 1.19 Å.[31] The coordinates for $B_{13}H_{19}$ were taken directly from the crystal structure.[6] The coordinates for $B_{14}H_{20}$ were taken from the crystal structure,[7] and then averaged to C_{2v} symmetry. For $B_{16}H_{20}$,[8] the crystal structure coordinates were used, except that the bridging hydrogen between B_6 and B_7 was relocated to a more symmetrical position. The geometry for i-$B_{18}H_{22}$[10] was generated from the x-ray coordinates for the $B_9 \ldots B_{18}$ subunit by passing a C_2 axis through B_9 and B_{10}. The n-$B_{18}H_{22}$[9] molecule lies on a center of inversion in the crystal and thus the coordinates used possess C_i symmetry. Since $B_{20}H_{16}$[11] occupies a crystal site having symmetry S_4, the coordinates were generated from the x-ray results with this $\bar{4}$ axis. The ion[12] $B_{20}H_{18}^{2-}$ also occupies a crystal site at a center of inversion, and hence the coordinates for $B_{20}H_{18}^{2-}$ were generated from the crystal structure coordinates for $B_1 \ldots B_{10}$, giving a molecule in the 1, 10 apex form. For photo-$B_{20}H_{18}^{2-}$, we generated a molecule with C_{2h} symmetry by using an idealized $B_{10}H_{10}^{2-}$ geometry[3] for the B_{10} fragments. The bridge hydrogens together with the B_{10} fragments were located in the molecule using average angles and distances from the crystal structure.[13] In order to ascertain how this molecular structure compares with that from the crystal structure, we superimposed the coordinates for the borons in the idealized $B_{10}H_{10}^{2-}$ onto the crystal structure coordinates of the $B_1 \ldots B_{10}$ half of photo-$B_{20}H_{18}^{2-}$; after suitable rotations, maximum coincidence was found to yield an rms deviation in coordinates of 0.13 au.[32] Computing times on an IBM 360/91 are 126 s for $B_{13}H_{19}$, 189 s for $B_{14}H_{20}$, 220 s for $B_{16}H_{20}$, 314 s for n-$B_{18}H_{22}$ and i-$B_{18}H_{22}$, 391 s for $B_{20}H_{16}$, and 430 s for $B_{20}H_{18}^{2-}$ and photo-$B_{20}H_{18}^{2-}$.

Canonical Molecular Orbital Results

The results of the energy analysis are given in Table I along with the highest occupied MO (HOMO) and lowest

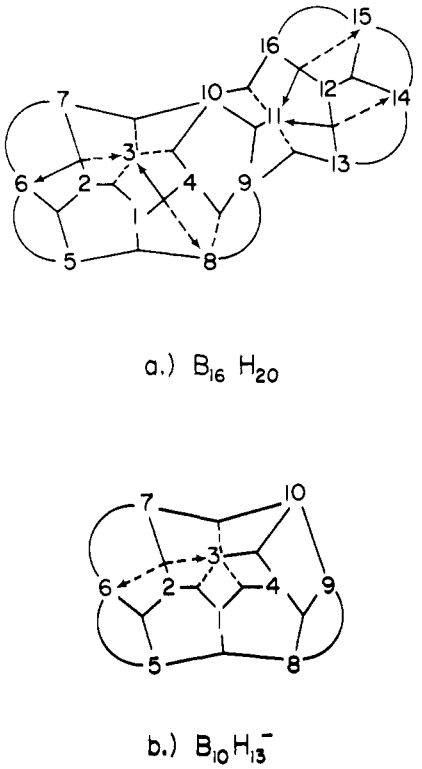

Figure 4. Localized valence structure for $B_{16}H_{20}$ and the related ion $B_{10}H_{13}^-$: (a) $B_{16}H_{20}$; (b) $B_{10}H_{13}^-$. Three-dimensional drawing for $B_{16}H_{20}$ is in ref 8.

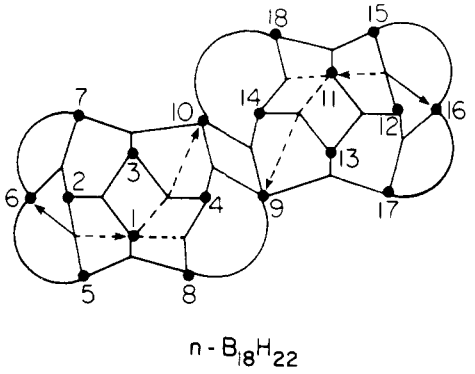

Figure 5. Localized valence structure for *n*-$B_{18}H_{22}$. Three-dimensional drawing is in ref 9.

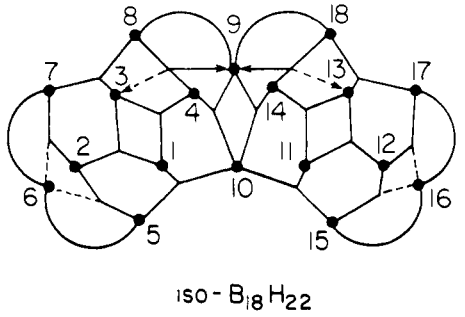

Figure 6. Localized valence structure for *i*-$B_{18}H_{22}$. Three-dimensional drawing is in ref 10.

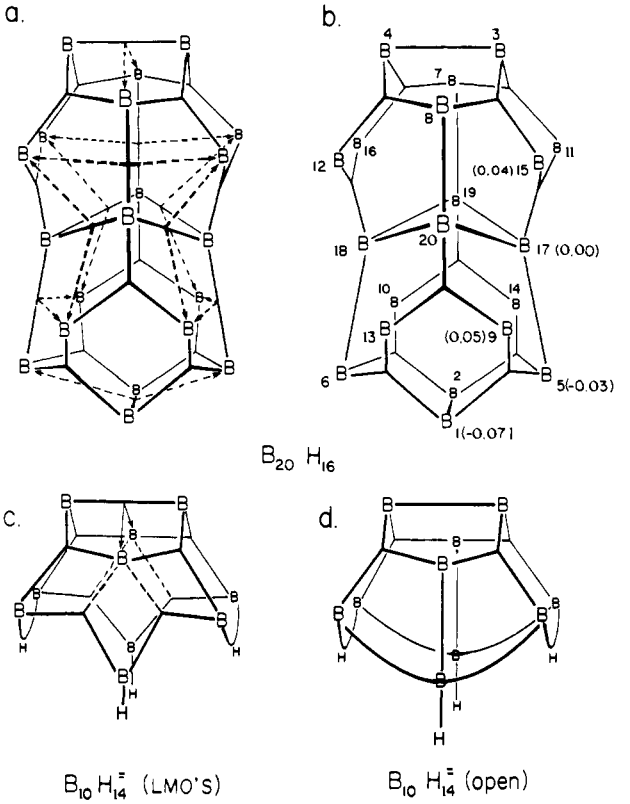

Figure 7. Localized valence structures for $B_{20}H_{16}$ and $B_{10}H_{14}^{2-}$. (a) Complete valence structure for $B_{20}H_{16}$ showing all bonding. (b) Simplified valence structure for $B_{20}H_{16}$ without delocalization arrows but with numbering and charges. (c) Boys LMO's for $B_{10}H_{14}^{2-}$. (d) Topological structure for $B_{10}H_{14}^{2-}$ with open three-center B-B-B bond.

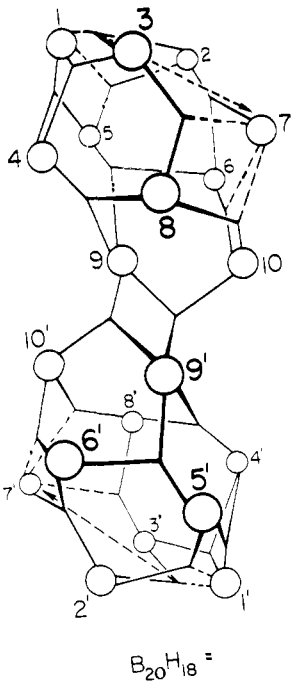

Figure 8. Localized valence structure for $B_{20}H_{18}^{2-}$.

unoccupied MO (LUMO) eigenvalues and the dipole moments. We find that *i*-$B_{18}H_{22}$ is more stable than *n*-$B_{18}H_{22}$, contrary to experiment,[19] but the small energy difference of 10 kcal/mol could easily be reversed upon geometry optimization. We feel that reasonable agreement with experiment is nevertheless obtained, because the experimental difference is only a few kilocalories per mole. For the isomers of $B_{20}H_{18}^{2-}$ we find that the photoisomer is calculated to be more stable than the normal isomer by 33 kcal/mol. Experimental evidence[20] suggests the opposite order of stability, since photo-$B_{20}H_{18}^{2-}$ is converted to $B_{20}H_{18}^{2-}$ by heating at 100 °C for 36 h. Again, these results cannot be used to

Table I. Energy Analysis[a]

	$B_{13}H_{19}$	$B_{14}H_{20}$	$B_{16}H_{20}$	n-$B_{18}H_{22}$	i-$B_{18}H_{22}$	$B_{20}H_{16}$	$B_{20}H_{18}^{2-}$	Photo-$B_{20}H_{18}^{2-}$
Nuclear repulsion energy	631.847	714.334	858.238	1043.386	1051.052	1182.476	1121.587	1148.232
Kinetic energy	331.852	356.844	406.361	456.698	4561.763	502.685	504.943	505.997
Nuclear attraction energy	−2023.822	−2245.571	−2647.898	−3133.454	−3148.699	−3518.283	−3438.988	−3492.798
Electron repulsion energy	728.580	817.570	977.025	1176.579	1184.077	1330.184	1308.438	1334.600
Total energy	−331.544	−356.823	−406.274	−456.791	−456.807	−502.937	−504.020	−503.968
Virial ratio ($-E/T$)	0.9991	0.9999	0.9998	1.002	1.0001	1.0005	0.9982	0.9960
Highest occupied[b] MO eigenvalue	−0.333	−0.361	−0.381	−0.371	−0.393	−0.430	−0.082	−0.085
Lowest unoccupied MO eigenvalue	0.085	0.028	0.035	0.010	0.018	−0.007 (2)	0.422	0.311
Dipole moment[c]	4.45	6.20	2.63	*d*	1.56	*d*	*e*	*e*

[a] All energies in atomic units (au). [b] For negative values, the absolute value corresponds to the ionization potential. [c] Units of debye. [d] Symmetric with no dipole moment. [e] The dipole moment of ions is origin dependent and is, therefore, not given.

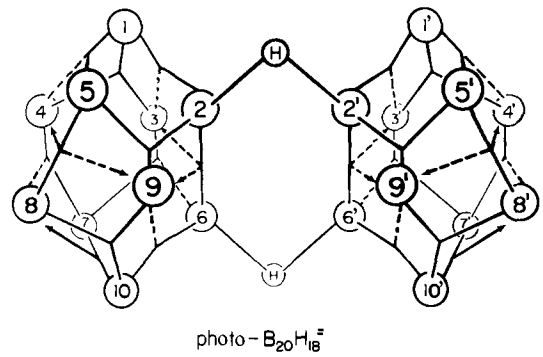

photo-$B_{20}H_{18}^{=}$

Figure 9. Localized valence structure for photo-$B_{20}H_{18}^{2-}$.

predict the order of stability without geometry optimization.

The HOMO eigenvalues of the $B_{20}H_{18}^{2-}$ ions are bound by more than 2 eV. As shown previously, only when the molecule becomes sufficiently large are the HOMO eigenvalues negative for dinegative boron ions at the minimum basis set level. We also note that the LUMO eigenvalue is very close to zero for all of the nonionic molecules, and for the large $B_{20}H_{16}$ molecule the degenerate LUMO pair is actually negative. For these large molecules, we then would expect electron addition to occur to form negative anions. As the number of heavy atoms in the molecule is increased, the accumulation of nuclear charge allows these large molecules to stabilize excess negative charge as compared with the lesser accumulation in smaller molecules.

Extensive use of static reactivity indices has been made in predicting the relative orders of electrophilic and nucleophilic attack in boron hydrides.[3,24] We have previously discussed such a treatment in some detail[24] and now apply it to the prediction of reactivity sites for the molecules in the present paper. We use inner-shell eigenvalues and group charges (Table II) as our major criteria for predicting the sites of attack. In order to choose one site over another, we shall insist upon a difference in inner-shell eigenvalue of at least 0.02 au and a difference in group charge of at least 0.02 to 0.03 e. The more positive eigenvalues and more negative group charges correlate with sites at which electrophilic attack tends to occur while negative eigenvalues and positive group charges correlate nucleophilic attack at that site.

In general, inner-shell eigenvalue and group charge predictions correlate extremely well with one another. However, for $B_{13}H_{19}$, this correlation is not as good. The most probable sites for electrophilic attack in this molecule are predicted to be 2 and 4 by both inner-shell eigenvalue and group charge. However, no simple prediction of the remaining order can be made based on our criteria, and a single choice as to the site of nucleophilic attack is not yet possible. The region of the molecule containing borons 3, 4, and 9 should be more susceptible to electrophilic attack according to our criteria, while the regions containing borons 11, 12, and 13 and boron 7 should be more susceptible to nucleophilic attack. The latter regions have most of the bridge hydrogens; we have previously predicted[24] that nucleophilic attack should occur at boron sites having bridge hydrogens.

In the series of molecules containing B_8H_{12} fragments, we noted that the predicted susceptibility of 4 and 5 to electrophilic attack increases markedly when the B_4-H_b-B_5 bridge hydrogen is replaced by either a pair of terminal hydrogens as in $B_8H_{13}^-$ or by the H-BH_2-H bridging group as in B_9H_{15}.[24] In $B_{13}H_{19}$, the B_7 fragment replaces the bridge hydrogen in B_8H_{12} but 4 and 5 now have different environments. Boron 4 in $B_{13}H_{19}$ is strongly bonded to a boron in the B_7 fragment and is more susceptible to electro-

Table II. PRDDO-SCF Inner-Shell Eigenvalues, Atomic Charges, and Group Charges

Molecule	Atom[a]	Eigenvalue[b]	Atomic charge[c]	Group charge[c]
$B_{13}H_{19}$	2	−7.542	−0.08	−0.15
	4	−7.526	−0.01	−0.13
	10	−7.571	−0.06	−0.12
	3	−7.578	0.00	−0.04
	9	−7.603	0.02	−0.04
	1	−7.594	0.06	0.00
	6	−7.612	0.05	0.01
	8	−7.642	0.05	0.05
	11	−7.657	0.04	0.05
	12	−7.681	0.07	0.06
	13	−7.671	0.08	0.08
	5	−7.648	0.08	0.10
	7	−7.667	0.12	0.12
$B_{14}H_{20}$	2(2′)	−7.575	−0.06	−0.12
	4(5)	−7.587	−0.02	−0.04
	1(1′)	−7.602	0.02	−0.02
	3(3′, 6, 6′)	−7.636	0.05	0.01
	7(7′, 8, 8′)	−7.694	0.10	0.08
$B_{16}H_{20}$	2	−7.564	−0.05	−0.12
	12	−7.576	−0.05	−0.12
	4	−7.585	0.00	−0.10
	1	−7.589	0.00	−0.06
	16	−7.609	−0.02	−0.05
	13	−7.616	−0.02	−0.04
	3	−7.601	−0.05	−0.02
	7	−7.620	0.03	−0.01
	5	−7.635	0.06	0.02
	10	−7.614	0.03	0.03
	9	−7.634	0.01	0.03
	11	−7.645	0.09	0.04
	8	−7.649	0.09	0.05
	6	−7.671	0.10	0.09
	14	−7.680	0.10	0.12
	15	−7.680	0.12	0.13
n-$B_{18}H_{22}$	2(12)	−7.573	−0.04	−0.12
	4(14)	−7.608	0.02	−0.07
	1(11)	−7.602	0.01	−0.05
	3(13)	−7.611	0.02	−0.04
	5(15)	−7.632	0.03	−0.01
	9(10)	−7.674	0.04	0.04
	7(17)	−7.637	0.03	0.05
	8(18)	−7.654	0.06	0.11
	6(16)	−7.683	0.13	0.13
n-$B_{18}H_{22}$	2(12)	−7.573	−0.04	−0.12
	4(14)	−7.613	0.01	−0.07
	3(13)	−7.603	0.00	−0.05
	1(11)	−7.608	0.03	−0.02
	7(17)	−7.640	0.04	0.00
	8(18)	−7.645	0.03	0.00
	5(15)	−7.630	0.04	0.02
	10	−7.656	0.07	0.07
	6(16)	−7.683	0.14	0.14
	9	−7.714	0.14	0.14
$B_{20}H_{16}$	1(2, 3, 4)	−7.603	0.00	−0.07
	5(6, 7, 8)	−7.622	0.03	−0.03
	17(18, 19, 20)	−7.679	0.00	0.00
	13(14, 15, 16)	−7.659	0.09	0.04
	9(10, 11, 12)	−7.659	0.10	0.05
$B_{20}H_{18}^{2-}$	1(1′)	−7.244	−0.08	−0.22
	7(7′)	−7.274	−0.10	−0.22
	3(3′)	−7.282	0.01	−0.13
	4(4′)	−7.290	0.02	−0.10
	2(2′)	−7.292	0.05	−0.10
	6(6′)	−7.297	0.01	−0.09
	10(10′)	−7.302	−0.04	−0.09
	5(5′)	−7.287	0.04	−0.08
	8(8′)	−7.294	0.03	−0.07
	9(9′)	−7.372	0.10	0.10
photo-$B_{20}H_{18}^{2-}$	1(1′, 10, 10′)	−7.251	−0.04	−0.18
	4(4′, 8, 8′)	−7.273	−0.01	−0.16
	5(5′, 7, 7′)	−7.284	0.00	−0.14
	3(3′, 9, 9′)	−7.294	0.02	−0.10
	2(2′, 6, 6′)	−7.363	0.06	−0.08

[a] Numbers in parentheses correspond to equivalent centers. [b] Units are atomic units (au). [c] Charges are in electrons (e).

philic attack. However, a terminal hydrogen on boron 5 is converted to a bridge hydrogen and boron 5 gains two near boron neighbors as a consequence of the addition of the B_7 fragment. Boron 5 is expected to be more susceptible to electrophilic attack than nucleophilic attack both here and in B_8H_{12}.

For $B_{14}H_{20}$, extremely good correlation between inner-shell eigenvalues and group charges is found. We predict that the order for electrophilic attack is 2 > 4 > 1 > 3 > 7. This order is identical with that predicted[24] for B_9H_{15} and $B_8H_{13}^-$. Again we point out that 4 is predicted to be much more susceptible to electrophilic attack than in B_8H_{12}, and in $B_{14}H_{20}$ two borons are bound to 4 instead of a bridge hydrogen as in B_8H_{12}.

For $B_{16}H_{20}$, borons 2, 12, 4, and 1 are predicted to be the likely sites of electrophilic attack while nucleophilic attack should most likely occur at 6, 14, and 15. Comparison with B_8H_{12} and $B_{10}H_{14}$[24] shows that the most probable sites of electrophilic and nucleophilic attack are retained in the corresponding fragments of $B_{16}H_{20}$ except that 10 has become much less susceptible to nucleophilic attack. Comparison with $B_{10}H_{13}^-$ shows[24] that 10 is much less susceptible to electrophilic attack in $B_{16}H_{20}$ than in $B_{10}H_{13}^-$ due, in part, to its being bound to two extra borons in the larger molecule. Boron 9 occupies an intermediate position in that it is susceptible to neither sort of attack in either $B_{16}H_{20}$ or $B_{10}H_{13}^-$, while the rest of the sites in $B_{16}H_{20}$ are very similar to those in $B_{10}H_{13}^-$.

We also have compared the B_8 fragment in $B_{16}H_{20}$ with those in several other systems. Borons 13 and 16 are quite susceptible to electrophilic attack in $B_{16}H_{20}$, just as in B_8H_{12}. On the other hand, 9 and 10 are quite different from the corresponding sites in most other B_8 molecules, more closely resembling 4 in B_8H_{12} and 5 in $B_{13}H_{19}$ in not being susceptible to electrophilic attack. Borons 5 and 6 in $B_{16}H_{20}$ are also similar to 5 in $B_{13}H_{19}$ because they too do not possess terminal hydrogens.

The reactivity orders for electrophilic attack for *n*-$B_{18}H_{22}$ and *i*-$B_{18}H_{22}$ are predicted to be 2 > 4, 3, 1 > 5, 7 > 9 > 8 > 6 and 2 > 4, 3, 1 > 7, 8, 5 > 10 > 6, 9, respectively. (The numbering in the $B_{18}H_{22}$ molecules is not identical, because borons 8 and 10 occupy different sites in the two molecules, as shown in Figures 5 and 6.) In both molecules, 2 is the site predicted to be most susceptible to electrophilic attack while 6 is predicted to be most susceptible to nucleophilic attack, just as found previously for $B_{10}H_{14}$. As in $B_{10}H_{14}$, atoms not attached to bridge hydrogens are the next most susceptible to electrophilic attack. A consequence of replacing the bridge hydrogen with a boron group is to lower the susceptibility of 4 to electrophilic attack.

In *n*-$B_{18}H_{22}$, we note that 8 is more susceptible to nucleophilic attack than is boron 9, which is located in the fusion region. In *i*-$B_{18}H_{22}$, this trend is reversed and the fusion borons 9 and 10 are more susceptible to nucleophilic attack than is 8. In *i*-$B_{18}H_{22}$, the fusion boron 9 which has two bridge hydrogens is more susceptible to nucleophilic attack than is the fusion boron 10 which has no bridge hydrogens. Because 10 has no terminal hydrogens, it may also be less susceptible to nucleophilic attack for steric reasons.

Experimentally, base-catalyzed D exchange occurs in *n*-$B_{18}H_{22}$ at two terminal hydrogens. We predict the equivalent sites 6 and 16 (the most positively charged) to be the most likely sites of exchange, in agreement with results obtained by Hawthorne and co-workers.[17] Electrophilic D exchange occurs at three pairs of positions, with one pair exchanging the most rapidly. We predict this pair to be 2 and 12, as did Hawthorne and co-workers,[17] who predicted the other two pairs to be 4 and 14 and 1 and 11 or 3 and 13 based on comparison with $B_{10}H_{14}$ and charge distributions from the counting of topological structures. However, our criteria do not distinguish between these additional sites in

their relative susceptibility to electrophilic attack. It is therefore likely that steric factors may play a role in these displacements.

Hawthorne and co-workers found that nucleophilic substitution does not occur for the isomers of $B_{18}H_{22}$ when acetonitrile is employed as the attacking agent.[17] However, Sneath and Todd[33] later reported nucleophilic substitution of cyclohexyl isocyanide with *i*-$B_{18}H_{22}$ and of pyridine with *n*-$B_{18}H_{22}$. In *n*-$B_{18}H_{22}$, two pyridines are added with loss of two hydrogens, and we expect that this substitution, in analogy with substitution in $B_{10}H_{14}$, should occur at 6 and 16. In *i*-$B_{18}H_{22}$, the addition compound $B_{18}H_{20}CNH_2C_6H_{11}$ is formed but we cannot predict the site for substitution except that it should occur at 6(16) or 9. The charge criteria are ambiguous but the inner-shell eigenvalue criterion does favor 9. Boron 9 is not completely blocked sterically because it has two bridge hydrogens which might open upon nucleophilic substitution. Still, it is clear experimentally that the $B_{18}H_{22}$ isomers are less susceptible to nucleophilic attack than is $B_{10}H_{14}$.

For $B_{20}H_{16}$, we predict 1 to be the most probable site for electrophilic attack, while 5 is the next most likely site. The order for nucleophilic attack is complicated somewhat because the four equivalent borons (17-20) do not possess hydrogens. Borons 9 and 13, which have terminal hydrogens, are clearly favored as the sites for nucleophilic attack by the charge criterion, but the eigenvalue criterion favors 17, which carries no terminal hydrogen. Borons 9 and 13 should be equivalent in the presumed D_{2d} structure of the free molecule even though they are not equivalent in the crystal structure due to the S_4 symmetry; they do show equivalent charges and eigenvalues as expected for a D_{2d} structure. The parent fragment for $B_{20}H_{16}$ is $B_{10}H_{14}^{2-}$. Boron 6 in $B_{10}H_{14}^{2-}$ (equivalent to 17 in $B_{20}H_{16}$) is most susceptible to electrophilic attack while 1 in $B_{10}H_{14}^{2-}$ is the next most susceptible.[24] Terminal hydrogens on 17 are not present in $B_{20}H_{16}$, and thus the emergence of 1 as the most probable site for electrophilic attack is reasonable, because it still has a terminal hydrogen. Boron 5 on $B_{20}H_{16}$ has become much more susceptible to electrophilic attack than is the comparable site, 2, in $B_{10}H_{14}^{2-}$.

We now compare the isomers of $B_{20}H_{18}^{2-}$ with the closo $B_{10}H_{10}^{2-}$ ion, in which electrophilic attack is expected at the apices (1) while nucleophilic attack is expected at the equatorial borons (2).[3] The charge and eigenvalue criteria agree that electrophilic attack should occur in $B_{20}H_{18}^{2-}$ at 1 and 7, while nucleophilic attack should occur at 9. Thus, for $B_{20}H_{18}^{2-}$, the apex *not* involved in bridging is one of the predicted sites of electrophilic attack, while the apex involved in the bridging is of intermediate reactivity. Even though 7 is an "equatorial" atom, it has a unique position opposite 9 and has become an important site of electrophilic attack, while 9, which is involved in bridging, has been singled out as the dominant site for nucleophilic attack.

In photo-$B_{20}H_{18}^{2-}$, electrophilic attack should occur at 1 while nucleophilic attack should occur at 2. As in $B_{20}H_{18}^{2-}$, the bridging borons which have no terminal hydrogens are expected to be the most susceptible to nucleophilic attack even though the bridging is quite different in the two molecules.

Localized Molecular Orbitals

Method. In previous work, we have discussed the procedures for obtaining Boys LMO's in some detail.[24,25] Briefly, we perform a unitary transformation on the canonical molecular orbitals (CMO) which maximizes D, the sum of squares (SOS),

$$D = \sum_{i=1}^{n} \langle \phi_i | \vec{r} | \phi_i \rangle \langle \phi_i | \vec{r} | \phi_i \rangle$$

Table III. Least Well-Determined LMO's

Molecule	Highest 2d[a] derivative eigenvalue, ν_{max}	Principally involved LMO's in ν_{max} eigenector
$B_{13}H_{19}$	−4.37	2-8-7, 2-3-1, 2-6-1
$B_{14}H_{20}$	−3.58	2-8-7, 2-3-1, 2-6-1, 2′-8′-7′, 2′-3′-1′, 2′-6′-1′
$B_{16}H_{20}$	−3.02	1-2-3, 2-7, 2-5-6, 10-4-3, 4-9-8, 1-4
i-$B_{18}H_{22}$	−1.35[b]	2-6-7, 2-5-6, 1-2-3 (2′-6′-7′, 2′-5′-6′, 1′-2′-3′)
n-$B_{18}H_{22}$	−1.99	10-9-4, 10-9-14, 1-4-8, 11-14-18, 1-3-4, 11-13-14
$B_{20}H_{16}$	−5.40[c]	3-4, 4-8-12, 4-7-16, 3-8-15, 3-7-11, 1-2, 1-6-13, 1-5-9, 2-5-14, 2-6-13
$B_{20}H_{18}^{2-}$	−4.60[b]	5-2-1, 3-2-1, 3-4-1, 8-3-7, 2-6-7 (15-12-11, 13-12-11, 13-14-11, 18-13-17, 12-16-17)
Photo-$B_{20}H_{18}^{2-}$	−1.47[d]	2-9-5, 3-6-7, 4-7-8, 5-1-4, 5-8, 7-10

[a] Inner shells were not included in the limited second-derivative test. [b] There are two degenerate eigenvectors. The other eigenvector corresponds to that composed of the bonds given in parentheses. [c] There are two degenerate eigenvectors. The second eigenvector just has a different phase from the first. [d] There are two degenerate eigenvectors of which only the unprimed one is given. The other corresponds to that given with primes on all numbers.

The two-orbital transformation procedure suggested by Edmiston and Ruedenberg[27] is used to apply the unitary transformation to the occupied molecular orbitals of the determinantal wave function.

Convergence for these molecules is quite slow. Since most localizations are unambiguous after 20 iterations, we report results after 20 iterations unless otherwise noted. In order to examine the uniqueness of the maxima, each localization was repeated at least ten times starting from different sets of MO's generated by a random unitary transformation of the initial CMO's. In order to determine whether the LMO's correspond to a maximum on the SOS surface, we perform a limited second-derivative test[25] in order to analyze the curvature of the LMO hypersurface. Such a test is of great value in examining whether multiple maxima are present on the surface. A relative maximum is reached on the SOS surface if the gradient vanishes and all eigenvalues of the second-derivative matrix are negative. In those cases (notably photo-$B_{20}H_{18}^{2-}$) which are not handled well by the two-orbital transformation procedure, we use a multiorbital transformation procedure designated as the eigenvector procedure.[25] The eigenvector procedure uses the eigenvector corresponding to the most positive eigenvalue of the second-derivative test to generate the unitary transformation. The largest second-derivative eigenvalues, ν_{max}, and the LMO pairings principally involved in the corresponding ν_{max} eigenvectors are given for the LMO structures in Table III. The ν_{max} eigenvectors give the directions of least negative curvature (ν_{max}) on the SOS surface.

$B_{13}H_{19}$. The LMO's for $B_{13}H_{19}$ are drawn in Figure 2a using previously described[24] conventions for drawing the bonds which for convenience are repeated in the legend for Figure 1. Examination of the region of the B_8 fragment shows at once the similarity to B_8H_{12} (Figure 1a). The major change in the B_8 fragment is that the 1-2-3 bond in $B_{13}H_{19}$ has more density on 1 than does the analogous bond in B_8H_{12}. The 4-5-1 bond shows substantial bonding to 1. Hence this fragment shows bonding more nearly like that in B_8H_{12} than like that in B_9H_{15} (Figure 2b), where the bonding to 1 is better represented as delocalization from the 4-5 two-center bond. The ν_{max} eigenvector for $B_{13}H_{19}$ (Table

Table IV. Atomic Coordinates

Atom	x, au	y, au	z, au
		$B_{13}H_{19}$	
B1	1.831 35	2.263 59	6.077 07
B2	0.282 67	1.528 53	6.577 72
B3	1.372 81	0.702 31	5.365 75
B4	3.085 85	1.161 53	5.660 24
B5	3.143 15	2.013 55	7.133 49
B6	1.399 96	2.195 23	7.801 62
B7	0.452 35	0.712 19	8.080 87
B8	0.380 03	−0.167 90	6.580 26
B9	3.785 02	0.291 45	7.000 41
B10	4.331 02	1.335 10	8.406 04
B11	4.422 92	3.015 15	7.966 35
B12	5.880 15	2.014 66	8.072 66
B13	5.492 53	0.385 03	7.556 96
H1	1.721 69	3.304 04	5.510 03
H2	−0.684 84	2.147 48	6.266 39
H3	1.017 41	0.621 30	4.232 95
H4	3.778 66	1.372 04	4.715 90
H6	1.199 59	3.131 04	8.508 88
H7	−0.330 87	0.578 70	8.966 78
H8	−0.475 13	−0.955 82	6.327 19
H9	3.255 29	−0.683 65	7.430 11
H10	4.037 34	1.051 64	9.523 85
H11	4.320 56	3.935 20	8.714 11
H12	6.732 29	2.316 91	8.846 35
H13	6.066 99	−0.568 02	7.978 63
H3-8	1.463 13	−0.396 50	5.881 84
H7-8	0.885 43	−0.454 72	7.631 21
H6-7	1.588 25	1.136 90	8.505 51
H5-11	3.866 54	3.156 81	6.937 29
H12-11	5.575 36	2.995 47	7.378 35
H12-13	6.197 79	1.361 87	7.057 47
H9-13	4.926 93	0.109 77	6.453 44
		$B_{14}H_{20}$	
B1	1.474	0.0	0.055
B1′	−1.474	0.0	0.055
B2	2.167 5	0.0	1.399 5
B2′	−2.167 5	0.0	1.399 5
B3	1.524	−1.422 5	1.079
B3′	−1.524	−1.422 5	1.079
B4	0.0	−0.957	0.0
B5	0.0	0.957	0.0
B6	1.524	1.422 5	1.079
B6′	−1.524	1.422 5	1.079
B7	1.973	0.877 5	2.740 5
B7′	−1.973	0.877 5	2.740 5
B8	1.973	−0.877 5	2.740 5
B8′	−1.973	−0.877 5	2.740 5
H1	2.088 1	0.0	−0.964 3
H1′	−2.088 1	0.0	−0.964 3
H2	3.784 6	0.0	1.171 7
H2′	−3.784 6	0.0	1.171 7
H3	1.949	−2.496 5	0.792 5
H4	0.0	1.615 8	−0.990 9
H5	0.0	−1.615 8	−0.990 9
H6	1.949	2.496 5	0.792 5
H6′	−1.949	2.496 5	0.792 5
H7	2.518 2	1.559 1	3.549 4
H7′	−2.518 2	1.559 1	3.549 4
H8	2.518 2	−1.559 1	3.549 4
H8′	−2.518 2	−1.559 1	3.549 4
H3-8	0.987	−1.475	2.194
H3′-8′	−0.987	−1.475	2.194
H7-8	1.252 5	0.0	3.355 5
H7′-8′	−1.252 5	0.0	3.355 5
H7-6	0.987	1.475	2.194
H7′-6-	−0.987	1.475	2.194
		$B_{16}H_{20}$	
B1	6.786 79	2.619 41	7.899 68
B2	7.170 01	−0.413 30	6.447 83
B3	5.824 51	2.144 09	4.706 85
B4	6.844 80	5.163 89	5.773 61
B5	9.569 93	0.898 99	8.390 88
B6	10.249 11	−0.927 36	5.655 06
B7	8.153 63	0.232 50	3.298 53
B8	9.434 56	4.667 92	7.862 37
B9	9.863 16	5.618 54	7.400 63
B10	7.957 70	3.820 61	2.909 92
B11	10.506 86	5.274 97	1.548 22
B12	9.756 43	8.077 78	−0.202 08
B13	10.940 19	8.320 61	3.021 84
B14	8.577 58	10.405 27	1.753 41
B15	6.561 95	8.635 75	−0.093 27
B16	7.595 15	5.414 46	−0.111 92
H1	5.334 08	2.859 56	9.600 38
H2	5.826 42	−2.107 05	7.069 37
H3	3.706 59	1.904 00	3.987 71
H4	5.423 50	6.895 52	5.978 00
H5	10.117 39	0.182 96	10.451 94
H6	11.525 77	−2.779 16	5.618 44
H7	7.760 26	−0.999 55	1.457 96
H8	10.050 00	5.924 39	9.623 87
H11	12.249 46	4.089 33	0.762 10
H12	10.958 73	8.639 91	−2.018 36
H13	12.923 74	9.273 49	3.488 67
H14	8.860 18	12.634 00	1.638 26
H15	5.264 80	9.484 42	−1.723 46
H16	7.104 99	4.573 81	−2.140 08
H5-6	11.472 84	0.671 66	6.932 81
H7-6	10.437 72	0.378 50	3.544 13
H8-9	11.449 36	4.515 20	6.307 40
H13-14	9.240 53	9.557 97	4.103 73
H15-14	6.233 57	9.790 46	2.020 77
H15-16	5.724 46	6.354 76	0.746 13
		n-$B_{18}H_{22}$	
B1	1.801 25	3.720 08	3.078 51
B2	3.161 92	1.418 49	5.105 67
B3	3.647 58	1.226 31	1.761 77
B4	1.178 29	2.681 38	−0.014 29
B5	−0.063 52	2.412 25	5.501 71
B6	0.956 98	−0.757 28	6.081 49
B7	2.954 95	−1.564 89	3.494 97
B8	−1.360 67	3.312 84	2.133 32
B9	−1.573 79	0.722 96	−0.128 61
B10	1.573 79	−0.722 96	0.128 61
B11	−1.801 25	−3.720 08	−3.078 51
B12	−3.161 92	−1.418 49	−5.105 67
B13	−3.647 58	−1.226 31	−1.761 77
B14	−1.178 29	−2.681 38	0.014 29
B15	0.063 52	−2.412 25	−5.501 71
B16	−0.956 98	0.757 28	−6.081 49
B17	−2.954 95	1.564 89	−3.494 97
B18	1.360 67	−3.312 84	−2.133 32
H1	2.606 45	5.772 05	3.527 36
H2	4.877 13	2.026 81	6.427 93
H3	5.723 79	1.473 92	0.932 07
H4	1.683 56	3.904 90	−1.833 11
H5	−0.927 67	3.639 37	7.177 34
H6	0.666 87	−1.889 77	8.003 38
H7	4.456 59	−3.236 48	3.600 88
H8	−2.820 48	4.980 15	1.746 76
H11	−2.606 45	−5.772 05	−3.527 36
H12	−4.877 13	−2.026 81	−6.427 93
H13	−5.723 79	−1.473 92	−0.932 07
H14	−1.683 56	−3.904 90	1.833 11
H15	0.927 67	−3.639 37	−7.177 34
H16	−0.666 87	1.889 77	−8.003 38
H17	−4.456 59	3.236 48	−3.600 88
H18	+2.820 48	−4.980 15	−1.746 76
H5-6	−1.290 99	0.320 31	5.409 85
H7-6	1.004 11	−2.425 13	4.266 63
H15-16	1.290 99	−0.320 31	−5.409 85
H17-16	−1.004 11	2.425 13	−4.266 63
H8-9	−2.602 48	1.052 42	2.000 62
H18-10	2.602 48	−1.052 42	−2.000 62
		i-$B_{18}H_{22}$	
B1	−2.722 88	−1.675 58	−2.699 14
B2	−2.316 75	−5.040 31	−2.605 34
B3	−0.013 57	−3.099 96	−4.061 64
B4	0.181 32	0.0	−2.886 44

Table IV (*Continued*)

Atom	x, au	y, au	z, au
B5	−3.408 54	−3.320 91	0.071 08
B6	−1.352 04	−5.992 06	0.349 87
B7	0.990 33	−5.515 92	−2.026 15
B8	2.684 54	−2.244 79	−2.335 87
B9	1.694 92	0.0	0.0
B10	−1.694 92	−0.000 01	0.000 01
B11	−2.722 88	1.675 58	2.699 14
B12	−2.316 75	5.040 31	2.605 34
B13	−0.013 57	3.099 96	4.061 64
B14	0.181 32	0.0	2.886 44
B15	−3.408 54	3.320 91	−0.071 08
B16	−1.352 04	5.992 06	−0.349 87
B17	0.990 33	5.515 92	2.026 15
B18	2.684 54	2.244 79	2.335 87
H1	−4.459 11	−0.755 45	−3.794 23
H2	−3.708 31	−6.368 18	−3.771 84
H3	0.461 30	−3.381 67	−6.242 35
H4	0.394 27	1.822 98	−4.187 11
H5	−5.425 62	−3.338 68	1.066 77
H6	−1.892 63	−7.859 70	1.481 27
H7	2.104 07	−7.319 22	−2.779 88
H8	4.681 16	−2.187 76	−3.370 57
H11	−4.459 11	0.755 45	3.794 23
H12	−3.708 31	6.368 18	3.771 84
H13	0.461 30	3.381 67	6.242 35
H14	0.394 27	−1.822 98	4.187 11
H15	−5.425 63	3.338 68	−1.066 77
H16	−1.892 63	7.859 70	−1.481 27
H17	2.104 07	7.319 22	2.779 88
H18	4.681 16	2.187 76	3.370 57
H5-6	−2.050 92	−3.964 85	1.755 29
H7-6	1.101 71	−5.488 09	0.397 16
H15-16	−2.050 92	3.964 85	−1.755 29
H17-16	1.101 71	5.488 09	−0.397 11
H8-9	3.045 75	−2.234 05	0.048 60
H18-9	3.045 75	2.234 05	0.048 60
		$B_{20}H_{16}$	
B1	1.227 25	1.130 61	−5.035 38
B2	−1.227 27	−1.130 62	−5.035 38
B3	−1.130 61	1.227 27	5.035 38
B4	1.130 62	−1.227 25	5.035 38
B5	−1.834 51	1.998 62	−3.808 74
B6	1.834 50	−1.998 63	−3.808 74
B7	−1.998 62	−1.834 51	3.808 74
B8	1.998 63	1.834 52	3.808 74
B9	1.037 61	3.231 36	−2.374 87
B10	−1.037 61	−3.231 37	−2.374 87
B11	−3.231 36	1.037 61	2.374 87
B12	3.231 37	−1.037 60	2.374 87
B13	3.302 48	0.744 02	−2.386 07
B14	−3.302 48	−0.744 02	−2.386 07
B15	−0.744 01	3.302 48	2.386 07
B16	0.744 02	−3.302 48	2.386 07
B17	−1.539 09	1.674 03	−0.504 10
B18	1.539 09	−1.674 03	−0.504 10
B19	−1.674 04	−1.539 09	0.504 10
B20	1.674 04	1.539 09	0.504 10
H1	2.087 70	1.947 74	−6.946 48
H2	−2.087 72	−1.947 75	−6.946 48
H3	−1.947 73	2.087 71	6.946 48
H4	1.947 75	−2.087 70	6.946 48
H5	−3.077 91	3.578 21	−4.818 31
H6	3.077 90	−3.578 22	−4.818 31
H7	−3.578 21	−3.077 90	4.818 31
H8	3.578 23	3.077 91	4.818 31
H9	1.106 45	5.478 52	−2.451 77
H10	−1.106 47	−5.478 53	−2.451 77
H11	−5.478 52	1.106 45	2.451 77
H12	5.478 53	−1.106 46	2.451 77
H13	5.544 48	0.609 12	−2.261 10
H14	−5.544 48	−0.609 12	−2.261 10
H15	−0.609 11	5.544 48	2.261 10
H16	0.609 11	−5.544 47	2.261 10
		p-$B_{20}H_{18}^{2-}$	
B1	−4.249 09	0.0	3.484 59
B2	−1.928 17	0.961 36	1.422 09
B3	−3.287 73	−2.320 92	1.422 09
B4	−6.570 01	−0.961 36	1.422 09
B5	−5.210 45	2.320 92	1.422 09
B6	−1.928 17	−0.961 36	−1.422 09
B7	−5.210 45	−2.320 92	−1.422 09
B8	−6.570 01	0.961 36	−1.422 09
B9	−3.287 73	2.320 92	−1.422 09
B10	−4.249 09	0.0	−3.484 59
B1′	4.249 09	0.0	3.484 59
B2′	1.928 17	0.961 36	1.422 09
B3′	3.287 73	−2.320 92	1.422 09
B4′	6.570 01	−0.961 36	1.422 09
B5′	5.210 45	2.320 92	1.422 09
B6′	1.928 17	−0.961 36	−1.422 09
B7′	5.210 45	−2.320 92	−1.422 09
B8′	6.570 01	0.961 36	−1.422 09
B9′	3.287 73	2.320 92	−1.422 09
B10′	4.249 09	0.0	−3.484 59
H1	−4.249 09	0.0	5.733 38
H3	−2.474 25	−4.284 83	2.155 83
H4	−8.533 91	−1.774 83	2.155 83
H5	−6.023 92	4.284 82	2.155 83
H7	−6.023 92	−4.284 82	−2.155 83
H8	−8.533 91	1.774 83	−2.155 83
H9	−2.474 25	4.284 83	−2.155 83
H10	−4.249 09	0.0	−5.733 38
H1′	4.249 09	0.0	5.733 38
H3′	2.474 25	−4.284 83	2.155 83
H4′	8.533 91	−1.774 83	2.155 83
H5′	6.023 92	4.284 82	2.155 83
H7′	6.023 92	−4.284 82	−2.155 83
H8′	8.533 91	1.774 83	−2.155 83
H9′	2.474 25	4.284 83	−2.155 83
H10′	4.249 09	0.0	−5.733 38
H2-12	0.0	1.658 47	2.851 37
H6-16	0.0	−1.658 47	−2.851 37
		$B_{20}H_{18}^{2-}$	
B1	11.541 54	3.146 69	4.345 37
B1′	14.100 39	−3.146 62	16.505 74
B2	10.804 80	−0.301 58	4.045 12
B2′	14.837 13	0.301 65	16.086 00
B3	14.037 34	1.314 13	3.949 20
B3′	11.604 59	−1.314 06	16.901 92
B4	13.468 01	3.149 57	6.824 57
B4′	12.173 92	−3.149 50	14.026 55
B5	10.034 00	1.800 99	6.826 66
B5′	15.607 93	−1.800 92	14.024 46
B6	10.599 13	−1.493 60	7.162 36
B6′	15.042 80	1.493 67	13.688 76
B7	13.264 68	−1.721 95	5.533 89
B7′	12.377 25	1.722 02	15.317 23
B8	15.285 49	0.321 74	6.991 38
B8′	10.356 44	−0.321 67	13.859 74
B9	12.461 77	0.774 13	9.043 13
B9′	13.172 20	−0.774 06	11.800 90
B10	13.624 63	−2.129 82	8.467 64
B10′	12.017 30	2.129 89	12.383 48
H1	10.272 82	4.636 59	3.230 42
H1′	15.369 11	−4.636 50	17.620 70
H2	9.339 84	−1.190 67	2.587 74
H2′	16.292 18	1.190 71	18.263 37
H3	15.616 77	1.488 98	2.356 97
H3′	10.025 16	−1.488 91	18.494 13
H4	14.681 00	4.712 01	7.895 94
H4′	10.960 93	−4.711 94	12.955 19
H5	8.122 80	2.606 77	7.697 52
H5′	17.519 10	−2.606 70	13.153 60
H6	17.138 93	2.753 64	13.170 83
H6′	8.712 93	−2.627 37	7.628 41
H7	14.015 39	−3.495 64	4.371 64
H7′	11.626 53	3.495 71	16.479 45
H8	17.501 88	0.694 33	7.086 96
H8′	8.140 03	−0.694 26	13.764 16
H10	14.672 65	−4.009 65	9.122 04
H10′	10.969 28	4.009 72	11.729 07

III) mixes the same LMO's as those which were mixed in B_8H_{12}.[24]

There are several ways to view the bonding in the remaining molecular fragment. This region is similar to that in $C_2B_4H_8$,[25] except that B-H_b-B bonds in $B_{13}H_{19}$ replace the B-C single bonds in $C_2B_4H_8$ and the C-C single bond which would connect 9 and 5 is now a 9-4 two-center bond to which 5 contributes weakly. The bonding in this fragment is not symmetric with respect to the local plane through 10 and 12, as the 10-11 single bond shows more two-center character than expected if the bonding in this fragment is analogous to that in $C_2B_4H_8$. Another, and new, comparison of this bonding region in $B_{13}H_{19}$ can be made to a hypothetical molecule, B_7H_{13}, shown in Figure 2c. Because all fused boranes are formed with a loss of two boron atoms, conceptually speaking, we therefore propose the structure in 2c as a candidate for the parent of the B_7 fragment in $B_{13}H_{19}$.

It is interesting to speculate on the relationship of the bonding to the atomic charges. We predicted that the region containing borons 3, 4, and 9 should be quite susceptible to electrophilic attack by our charge criteria. In agreement with this expectation, we find substantial charge density localized in this region as represented by the 4-9 bond and the 3-4-5 bond. The latter bond has most of its density on 3 and 4.

$B_{14}H_{20}$. $B_{14}H_{20}$ has C_{2v} symmetry, and the LMO structure (Figure 3) also exhibits this symmetry. The bonding in each fragment is essentially that in B_8H_{12} except that the necessarily symmetrical donation of the 4-5 bond to 1 and 1′ is lower in $B_{14}H_{20}$, being more like that in B_9H_{15}. The ν_{max} eigenvector (Table III) mixes bonds 2-8-7, 3-2, and 6-2 (and their primed counterparts), just as is found for B_8H_{12}.[24] In this molecule fusion does not substantially distort the bonding in the B_8 fragments, most probably because the two-center 4-5 bond in the fusion region can bond equally to 1 and 1′ through delocalization in a manner like that found in B_8H_{12} and B_9H_{15}.

$B_{16}H_{20}$. The $B_{16}H_{20}$ molecule has been discussed in a preliminary note.[28] Its LMO's are shown in Figure 4a. The B_8 region of this molecule has a bonding pattern identical with that found in B_8H_{12} (Figure 1a). Comparison of the bonding in the B_{10} fragment of $B_{16}H_{20}$ with that of $B_{10}H_{14}$ (Figure 1b) shows quite a large disparity. On the other hand, this region of bonding in $B_{16}H_{20}$ shows a striking qualitative similarity to that found for $B_{10}H_{13}^-$ (Figure 4b). Somewhat more delocalization on 6 from the 7-2 bond is seen in $B_{16}H_{20}$ while the 1-4-3 bond shows more population at 3 in $B_{10}H_{13}^-$ than in $B_{16}H_{20}$. Also, some delocalization of the 1-4 bond in $B_{16}H_{20}$ to 8 is evident. In going from $B_{10}H_{13}^-$ to $B_{16}H_{20}$ we note that the 4-9-8 bond has slightly decreased in population on 8 and the 10-4-3 bond has decreased in population on 3. It is thus evident that the removal of the proton from $B_{10}H_{14}$ to form $B_{10}H_{13}^-$ is similar to the addition of the B_8 fragment to the B_{10} fragment to form $B_{16}H_{20}$ in its effect on the LMO's. Examination of the ν_{max} eigenvector for $B_{16}H_{20}$ shows the identical orbital mixing found in $B_{10}H_{13}^-$, but not the orbital mixings found in B_8H_{12}. This reinforces our observation[24] that the LMO's in the central regions of molecules with a framework like that of $B_{10}H_{14}$ are among the least well-determined LMO's known.

***n*-$B_{18}H_{22}$.** The LMO structure for *n*-$B_{18}H_{22}$ (Figure 5) shows the inversion symmetry of the molecule. The two bonds that bridge the boron fragments are three-center bonds very similar to those found in $B_{10}H_{14}$. The bonding in the fragments themselves is somewhat similar to that found for $B_{10}H_{14}$ and $B_{10}H_{13}^-$. Actually the basic bonding pattern is that of $B_{10}H_{13}^-$ except that the bonding pattern is reflected through a line passing through 2 and 4, i.e., the bonding patterns at centers 1 and 3 are reversed from those in $B_{10}H_{13}^-$. If, as in $B_{16}H_{20}$, the bridging fragment simply replaced the single bond in $B_{10}H_{13}^-$, we would have expected 3 to be the fractional center in *n*-$B_{18}H_{22}$ rather than 1. Other than this reversal about the 2-4 line, the bonding is the same as that found for $B_{10}H_{13}^-$ except for the slight delocalization of the 3-4-1 bond to 10, which was also seen in $B_{16}H_{20}$.

The effect, therefore, of fusing the $B_{10}H_{14}$ fragment to $B_{10}H_{14}$ in the normal configuration is to cause the LMO's to undergo a distortion similar to that found in $B_{10}H_{13}^-$ but with the LMO's in a different region than expected. The fusion region does not have fractional bonds to 9 or 10 as found in $B_{10}H_{14}$ but has a more nearly equally apportioned three-center bond which appears to determine the remaining bonding pattern. An important result is that the 2-6-7 bond is thereby more equally apportioned. The consequences are that 1 becomes a fractional center, the 4-8-9 bond of $B_{10}H_{14}$ becomes a 4-8-1 bond in *n*-$B_{18}H_{22}$, and the 2-5-6 bond of $B_{10}H_{14}$ becomes a 2-5 bond being somewhat delocalized on 1 and 6.

***i*-$B_{18}H_{22}$.** Fusion of two $B_{10}H_{14}$ fragments in a different geometry as in *i*-$B_{18}H_{22}$ allows us to examine how the bonding patterns change with geometry. The LMO's for *i*-$B_{18}H_{22}$ are shown in Figure 6 and again the LMO structure shows the molecular symmetry, here C_2. In contrast to the results just noted for *n*-$B_{18}H_{22}$, we find the LMO's in *i*-$B_{18}H_{22}$ to be very similar to those found in $B_{10}H_{14}$. The only differences occur, as expected, in the fragment fusion region, where the 4-10-9 bond is not fractional to 9 as had been found in $B_{10}H_{14}$. As a consequence, the 4-8-9 bond has some population on 3, and 9 participates in the bond to a lesser extent (0.33 e) than in $B_{10}H_{14}$. Thus, introduction of the bridging fragment in *i*-$B_{18}H_{22}$ yields the same sort of bonding in the fusion region as found for *n*-$B_{18}H_{22}$ but the perturbation is not carried into the regions of the molecule removed from the fusion region to the same extent as in *n*-$B_{18}H_{22}$ and $B_{16}H_{20}$.

The ν_{max} eigenvector for *i*-$B_{18}H_{22}$ mixes the 2-6-7, 2-5-6, and 1-2-3 bonds, or only half of those mixed in the ν_{max} eigenvector of $B_{10}H_{14}$. For *n*-$B_{18}H_{22}$ the ν_{max} eigenvector mixes the corresponding three bonds found near the fusion region (Table III).

$B_{20}H_{16}$. The molecule $B_{20}H_{16}$ is a closo borane formed by the bridging of two open fragments. The LMO structure (Figure 7a) shows approximate D_{2d} symmetry. A simplified structure is shown in Figure 7b. The most striking feature of the bonding is the large number of essentially two-center bonds, as a result of which eight centers (9-16) have a total of only three bonds each. However, each of these eight centers contributes 0.22 e to each of two additional two-center bonds. Four other centers (5-8) are normal centers, each having four bonds, and each participating to the extent of 0.22 e in the cap bonds (1-2 and 3-4).

Comparison of the LMO's for $B_{20}H_{16}$ with those for $B_{10}H_{14}$ (Figure 1b) shows that the $B_{20}H_{16}$ fragment structures are not at all similar to those of $B_{10}H_{14}$. Instead, the pattern of LMO's shown by $B_{10}H_{14}^{2-}$ (Figure 7d) resembles that present in the upper and lower halves of $B_{20}H_{16}$. However, the bonding in $B_{20}H_{16}$ resembles more the topological structure which has an open three-center bond (Figure 7d) than the structure found by the Boys localization (Figure 7c). Bridging of the two $B_{10}H_{14}^{2-}$ groups to form $B_{20}H_{16}$ requires the loss of two terminal B-H_t bonds and the dissolution of an open three-center bond for each boron in the incipient central ring of four borons. Thus, there is a nominal addition of 2.67 at each of these four boron atoms. Two of these electrons go into forming the two two-center

bonds that fuse the two fragments. The remaining 0.67 e contributes to the formation of the other fusion bond, which connects each of these borons lacking terminal hydrogens to the two borons that lose a bridge hydrogen as H^- in forming a new three-center B-B-B bond (e.g., 9-13-20). The ν_{max} eigenvector for $B_{20}H_{16}$ mixes the cap single bonds with the four adjacent three-center B-B-B bonds. A similar mixing was noted in $B_{10}H_{14}^{2-}$.

We note that each of the boron atoms 9-16 having only three bonds are the most positive centers as determined by group and atomic charges. Further, the centers 5-8 are less negative than are centers 1-4, the centers involved in the bonds that donate to 5-8.

$B_{20}H_{18}^{2-}$. The two isomers of $B_{20}H_{18}^{2-}$ are the only known bridged boranes that are composed of closo borane subunits. The LMO's for these two isomers give striking confirmation of this relationship. The LMO structure for $B_{20}H_{18}^{2-}$ (Figure 8) shows C_i symmetry.

Before discussing the LMO's for this molecule, we shall first examine the bonding in the parent $B_{10}H_{10}^{2-}$ ion. The two localized structures for $B_{10}H_{10}^{2-}$ depicted in Figure 1d and Figure 1e are both relative maxima on the SOS surface. We denote them as 4,4,3 (Figure 1d) or 3,5,3 (Figure 1e) structures, depending on the number bonds which join the apices to the equatorial borons (the first and third integers) and the number joining the two equatorial rings (the second integer). Attempts to interconvert the two structures by following the ν_{max} eigenvector[25] in all cases lead instead to a symmetry related structure of the same type.

The LMO's of $B_{20}H_{18}^{2-}$ are essentially identical with those of the 4,4,3 structure for $B_{10}H_{10}^{2-}$ given in Figure 1d. The only change in the LMO's is that the 2-6-7 bond in $B_{20}H_{18}^{2-}$ is not fractionally populated on 7 as had been found in $B_{10}H_{10}^{2-}$ and the 2-5-1 bond is fractional to 1 in $B_{20}H_{18}^{2-}$. Even the delocalization of the 1-3-2 bond to 7 in $B_{10}H_{10}^{2-}$ is reproduced in $B_{20}H_{18}^{2-}$. The bridging between the two fragments is accomplished by two three-center bonds which replace the 9-10 and 9′-10′ bonds in $B_{10}H_{10}^{2-}$. Thus the only changes in going from two $B_{10}H_{10}^{2-}$ ions to $B_{20}H_{18}^{2-}$ are the formal loss of two hydride ions, and the formation of the two bridging three-center B-B-B bonds between the newly electron deficient centers from the precursor two-center B-B bonds.

The orbitals of the 4,4,3 structure for $B_{10}H_{10}^{2-}$ are arranged perfectly for the bonding in $B_{20}H_{18}^{2-}$ since the single bond (9-10) lies in the C_s plane of the $B_{10}H_{10}^{2-}$ LMO structure. The same plane is essentially retained in $B_{20}H_{18}^{2-}$, and the same bonding can and does occur. As we have noted before,[24] borons on the planes of symmetry that describe the LMO's are often fractional centers, for example in $B_{11}H_{13}^{2-}$ and $C_2B_5H_7$. The total wave function describing the LMO's has the correct molecular symmetry but in our figures using truncated LMO's, the apparent symmetry may be lower. We note that the fractional center 7 is also a very negative center according to its inner-shell eigenvalue and atomic charge in $B_{20}H_{18}^{2-}$.

Photo-$B_{20}H_{18}^{2-}$. The two B_{10} units of photo-$B_{20}H_{18}^{2-}$ are bound together by bridge hydrogens rather than via the boron bridging found in $B_{20}H_{18}^{2-}$. The LMO's for the photoisomer are shown in Figure 9. Here we find that the LMO structure is based on 3,5,3 $B_{10}H_{10}^{2-}$ subunits (Figure 1e). One slight variation in the $B_{10}H_{10}^{2-}$ bonding is that the apical-equatorial 7-10 single bond delocalizes away from the bridge hydrogen site 6 in photo-$B_{20}H_{18}^{2-}$, rather than equally to 8 and 6 as is in $B_{10}H_{10}^{2-}$. The two bonds having populations of less than 0.5 e to 7 in $B_{10}H_{10}^{2-}$ now show less bonding to 6 and 8 in $B_{20}H_{18}^{2-}$ with a concomitant rise in the populations of these bonds on 7. Also, less delocalization to 3 is found in $B_{20}H_{18}^{2-}$ than in $B_{10}H_{10}^{2-}$.

The LMO structures of the B_{10} fragments in photo-$B_{20}H_{18}^{2-}$ are related by a plane of symmetry. Five localizations (four from random starting points and one starting from the CMO's) were carried out. In two cases the C_s structure was found after 20 iterations. For the other localizations for $B_{20}H_{18}^{2-}$ it was necessary to use the eigenvector procedure in order to complete the localization. After a series of 20-2-10-3-5 (20 2 × 2 iterations, 2 eigenvector iterations, 10 2 × 2 iterations, etc.), the random starting structures yielded the C_s LMO structure. The final LMO structure obtained in this way from the highly delocalized CMO's was still not well converged. Even an additional 10-2-15-2-5 series of iterations did not achieve complete convergence, but the structure was definitely tending toward the C_s LMO structure. Thus, contrary to our original comment,[28] we do not find multiple maxima on the SOS localization surface for photo-$B_{20}H_{18}^{2-}$. This result clearly demonstrates the utility of the recently formulated eigenvector procedure in determining whether multiple maxima are present on the SOS surface.

Thus, the placement of the bridge hydrogens determines which set of the $B_{10}H_{10}^{2-}$ LMO's will occur in photo-$B_{20}H_{18}$, as had the joining by boron bridging in $B_{20}H_{18}^{2-}$. The LMO's are chosen so that a single bond is placed between borons that are attached to bridging hydrogens. Given these two bonds, the remaining LMO's fall into one of the equivalent symmetry orientations for the 3,5,3 $B_{10}H_{10}^{2-}$ subunits.

The molecular coordinates given in Table IV were added at the suggestion of a referee.

Acknowledgment. We wish to acknowledge support of this research by the Office of Naval Research. We thank R. Schaeffer and J. Huffman for sending us coordinates prior to publication. D.A.D. thanks the Parker Foundation for a fellowship.

References and Notes

(1) W. N. Lipscomb, "Boron Hydrides", W. A. Benjamin, New York, N.Y., 1963.
(2) W. N. Lipscomb, *Acc. Chem. Res.*, **6**, 257 (1973).
(3) J. H. Hall, Jr., D. S. Marynick, and W. N. Lipscomb, *J. Am. Chem. Soc.*, **96**, 770 (1974).
(4) (a) T. A. Halgren and W. N. Lipscomb, *J. Chem. Phys.*, **58**, 1569 (1973); (b) J. A. Pople and D. L. Beveridge, "Approximate Molecular Orbital Theory", McGraw-Hill, New York, N.Y., 1970.
(5) T. A. Halgren, D. A. Kleier, J. H. Hall, Jr., L. D. Brown, and W. N. Lipscomb, to be submitted.
(6) $B_{13}H_{19}$: J. C. Huffman, D. C. Moody, J. W. Rathke, and R. Schaefer, *J. Chem. Soc., Chem. Commun.*, 308 (1973); J. C. Huffman, private communication.
(7) $B_{14}H_{20}$: J. C. Huffman, D. C. Moody, and R. Schaeffer, *J. Am. Chem. Soc.*, **97**, 1621 (1975).
(8) $B_{16}H_{20}$: L. B. Friedman, R. E. Cook, and M. D. Glick, *Inorg. Chem.*, **9**, 1452 (1970). The angle β is incorrectly given in the paper and should be 79.17°.
(9) *n*-$B_{18}H_{22}$: P. G. Simpson and W. N. Lipscomb, *Proc. Natl. Acad. Sci. U.S.A.*, **48**, 1490 (1962); P. G. Simpson and W. N. Lipscomb, *J. Chem. Phys.*, **39**, 26 (1963).
(10) *i*-$B_{18}H_{22}$: P. G. Simpson, K. Folting, and W. N. Lipscomb, *J. Am. Chem. Soc.*, **85**, 1879 (1963); P. G. Simpson, K. Folting, R. D. Dobrott, and W. N. Lipscomb, *J. Chem. Phys.*, **39**, 2339 (1963).
(11) $B_{20}H_{16}$: R. D. Dobrott, L. B. Friedman, and W. N. Lipscomb, *J. Chem. Phys.*, **40**, 866 (1964).
(12) $B_{20}H_{18}^{2-}$: C. H. Schwalbe and W. N. Lipscomb, *Inorg. Chem.*, **10**, 15 (1971).
(13) Photo-$B_{20}H_{18}^{2-}$: B. G. DeBoer, A. Zalkin, and D. H. Templeton, *Inorg. Chem.*, **7**, 1085 (1968).
(14) R. L. Pilling, M. F. Hawthorne, and E. A. Pier, *J. Am. Chem. Soc.*, **86**, 3568 (1964).
(15) R. L. Pilling and M. F. Hawthorne, *J. Am. Chem. Soc.*, **88**, 3873 (1966).
(16) (a) L. B. Friedman, R. D. Dobrott, and W. N. Lipscomb, *J. Am. Chem. Soc.*, **85**, 3505 (1963); (b) N. E. Miller, J. A. Forstner, and E. L. Muetterties, *Inorg. Chem.*, **3**, 1690 (1964).
(17) F. P. Olsen, R. C. Vasavada, and M. F. Hawthorne, *J. Am. Chem. Soc.*, **90**, 3946 (1968).
(18) A. Kaczmarcyzk, R. D. Dobrott, and W. N. Lipscomb, *Proc. Natl. Acad. Sci. U.S.A.*, **48**, 729 (1962).
(19) A. R. Pitochelli and M. F. Hawthorne, *J. Am. Chem. Soc.*, **84**, 3218 (1962).

(20) M. F. Hawthorne and R. L. Pilling, *J. Am. Chem. Soc.*, **88**, 3873 (1966).
(21) H. R. Bachmann, H. Nöth, R. Rinek, and K. C. Kompa, *Chem. Phys. Lett.*, **29**, 627 (1974).
(22) J. Plesek, S. Hermanek, B. Stibrand, and F. Hanousek, *Collect. Czech. Chem. Commun.*, **32**, 1095 (1967); **33**, 699 (1968).
(23) J. Rathke and R. Schaeffer, *Inorg. Chem.*, to be published.
(24) J. H. Hall, D. A. Dixon, D. A. Kleier, T. A. Halgren, L. D. Brown, and W. N. Lipscomb, *J. Am. Chem. Soc.*, **97**, 4202 (1975).
(25) D. A. Kleir, T. A. Halgren, J. H. Hall, and W. N. Lipscomb, *J. Chem. Phys.*, **61**, 3905 (1974).
(26) (a) S. F. Boys, *Rev. Mod. Phys.*, **32**, 296 (1960); (b) J. M. Foster and S. F. Boys, *ibid.*, **32**, 300 (1960); (c) S. F. Boys, "Quantum Theory of Atoms, Molecules and the Solid State", P.-O. Löwdin, Ed., Academic Press, New York, N.Y., 1966, p 253.
(27) C. Edmiston and K. Ruedenberg, *Rev. Mod. Phys.*, **35**, 457 (1963).
(28) D. A. Dixon, D. A. Kleier, T. A. Halgren, and W. N. Lipscomb, *J. Am. Chem. Soc.*, **96**, 2293 (1974).
(29) D. A. Dixon, J. H. Hall, D. A. Kleier, T. A. Halgren, and W. N. Lipscomb, to be submitted.
(30) E. Switkes, R. M. Stevens, W. N. Lipscomb, and M. D. Newton, *J. Chem. Phys.*, **51**, 2085 (1969).
(31) T. A. Halgren, R. J. Anderson, D. S. Jones, and W. N. Lipscomb, *Chem. Phys. Lett.*, **8**, 547 (1971).
(32) T. A. Halgren, to be published.
(33) R. L. Sneath and L. J. Todd, U.S. National Technical Information Service, AD Rep. No. 745355 (1972); *Chem. Abstr.*, **77**, 172107w (1972).

Vibrational Spectra and Structure of Methylberyllium Borohydride

Louis J. Allamandola and Joseph W. Nibler*

Contribution from the Department of Chemistry, Oregon State University, Corvallis, Oregon 97331. *Received August 8, 1975*

Abstract: Vapor density measurements of unsaturated methylberyllium borohydride at 1.2 Torr show that this species is predominantly dimeric in the gas phase. It was found that the major features of the infrared spectrum of the annealed solid agree with those of the vapor, implying that the solid is made up of dimeric units also. Infrared and Raman spectra further show the borohydride moiety is attached to beryllium by a double hydrogen bridge. From comparison with Raman spectra of solid dimethylberyllium, known to contain only methyl bridges, it is concluded that methylberyllium borohydride contains two bridging methyl groups. The spectra are consistent with C_{2h} molecular symmetry and vibrational assignments of $(CH_3BeBH_4)_2$ and $(CH_3Be^{10}BD_4)_2$ are presented on this basis. Vibrations characteristic of BeH_2BH_2 and bridging methyl groups are identified and compared with analogous compounds. With the exception of the deformation modes, the methyl vibrations are generally quite close to those of terminal methyl groups. The deformation frequencies are significantly higher for bridged methyls and thus serve as a basis for identification of this type of bonding.

Recent studies of metal borohydrides have shown a variety of structures for these electron deficient compounds, with both double $[Al(BH_4)_3$,[1] $C_5H_5BeBH_4]$[2] and triple $[Be(BH_4)_2$,[3,4] $Zr(BH_4)_4$[5]] hydrogen bridges being observed. Perhaps the most unusual metal borohydride yet reported is $Be(BH_4)_2$, which is believed to exist in two vapor forms, one with double hydrogen bridges and a more stable linear C_{3v} form containing triple hydrogen bridges, HBH_3BeH_3BH. For the solid, however, x-ray[6] and spectroscopic[7] studies reveal a helical polymeric structure of linked ions: $\cdots (BH_4^-) \cdots (H_2BH_2Be^+) \cdots (BH_4^-) \cdots$. This borderline tendency of $Be(BH_4)_2$ toward an ionic structure is consistent with the fact that all the other group 2 (and group 1) borohydrides are ionic salts. Such unusual bonding and structural changes might well be expected for other metal borohydrides, and a number of those which are expected to lie between the ionic and covalent extremes have recently been investigated. One such compound is methylzinc borohydride which has been shown to convert from a double hydrogen bridged structure in the vapor phase to an ionic form $CH_3Zn^+ \cdots BH_4^-$ in the solid.[8] Similarly, $U(BH_4)_4$ is believed to change from a tetrahedral, triple-bridged vapor form to a polymeric ionic form involving both BH_4^- ions and double bridged (H_2BH_2U) units in the solid phase.[9]

At present a clear picture has not emerged as to which metal atom properties dominate in determining the structures (ionic or covalent) or the type of hydrogen bridging (double or triple) present in metal borohydrides. As part of a continuing effort in this direction, we report here the spectral investigation of a $Be(BH_4)_2$ derivative: methylberyllium borohydride, CH_3BeBH_4. The gas-phase infrared spectrum of this molecule has been reported previously by Cook and Morgan[10] and they concluded that the vapor consists of a mixture of monomer and methyl-bridged dimer. A freezing point depression experiment showed the molecule to be dimeric in benzene. In our study we have examined this equilibrium by vapor density measurements and by trapping the vapor at low pressure using matrix isolation techniques. Our intention was to obtain infrared and Raman spectra of both monomer and dimer but, as described below, it was not possible to obtain significant amounts of the monomer. Thus this report deals primarily with the spectrum and structure of dimeric CH_3BeBH_4 in the solid phase.

Experimental Section

The samples of CH_3BeBH_4, $CH_3Be^{10}BD_4$, and $(CH_3)_2Be$ were prepared by Dr. Thomas Cook and the syntheses have been described previously.[10] Since these compounds are pyrophoric and poisonous, all sample handling was done in a greaseless vacuum system in a hood. The vapor density at 24 °C was measured at two pressures using a Granville Phillips capacitance manometer and an inert oil (Halocarbon Products Corp., series 10-25) manometer. At saturation, 129.4 ± 0.5 mg of CH_3BeBH_4 gave a pressure of 5.6 ± 0.2 Torr in 5.7 ± 0.1 l., yielding a molecular weight of 75 ± 5 g/mol (mol wt CH_3BeBH_4 = 39 g/mol). At lower pressures, 25.2 ± 0.5 mg of $CH_3Be^{10}BD_4$ in a volume of 5.89 ± 0.06 l. gave a pressure of 1.2 ± 0.1 Torr, from which the molecular weight is 69 ± 8 g/mol (mol wt $CH_3Be^{10}BD_4$ = 42 g/mol). Thus the material is largely dimeric in the vapor phase even under nonsaturated conditions.

Infrared and Raman spectra of films sublimed onto a polished aluminum block cooled by a Displex closed cycle cooler were obtained as follows. The samples were annealed to about 200 K at least three times until the infrared spectra no longer changed. In-